

Chapter 2

Relating Small-Scale Emission and Concentration Variability in Air Quality Models

Stefano Galmarini, Jean-François Vinuesa, and Alberto Martilli

Abstract A novel approach to account for the spatial variability of the small-scale emission in air quality models is proposed. This approach includes a formulation for the sub-grid variability of pollutant concentrations and relates it to the spatial heterogeneity of the emissions. The parameterization is implemented in a 3D transport model and tested against large eddy simulations of convective atmospheric boundary layers.

2.1 Introduction

The atmospheric motion, evolution and scalar concentrations can be described by a system of non-linear partial differential equations. These equations are derived from thermodynamics and fluid mechanics (Navier-Stokes equations). They describe the characteristics of a given air mass and are the base of all geophysical models. They link large and small scale motions due to the wide range of temporal and spatial scales of geophysical processes and the energy feedback from smaller scales into the larger scale motions. Since the equations are simply too complicated to be exactly solved for any practical atmospheric modelling, statistical representations of the complete physical description is required. Currently, the Navier-Stokes equations are resolved by performing scale decomposition. Geophysical models are in fact an adaptation of these equations to a spatial grid and discrete steps in time. It is therefore important to realize that features smaller than the dimension of one grid cell cannot be resolved by the model. These are referred to as subgrid scale processes.

Urban and suburban environments are characterized by heterogeneous emissions. These are not reflected in emission inventories except as an average value and so this is not accounted for in meso/limited area air quality models. The emissions are

S. Galmarini (✉)

European Commission – DG Joint Research Centre, Institute for Environment and Sustainability,
TP 441, 21020 Ispra, Italy
e-mail: stefano.galmarini@jrc.it

averaged over the grid cell where the emission source is located. The source can be linear (e.g. roads), areal (fields or urban areas) or point (factory) but after the averaging procedure, it is considered as a surface source with the same extent as the grid cell. This means that not only is the surface heterogeneity lost in terms of its level of variability but also it will not be accounted for in the upper atmospheric levels and the impact of the spatial distribution of emissions on the spatial distribution of concentrations, is lost. This can represent a serious issue in the case of passive as well as chemically reactive species, or for the estimation of long- or short-term exposures.

Since this crucial component can be at smaller scales than the grid size, it could be accounted for through a sub-grid parameterization. In this paper, we propose a novel approach to this parameterization, including a formulation for the sub-grid variability of pollutant concentrations that takes into account the spatial heterogeneity of the emissions. The formulation that can be used in mesoscale models relies on the resolution of a prognostic equation for the sub-grid concentration variance, i.e. the quantity that accounts for the distribution of concentration within a grid-cell of a mesoscale model, by using a 1.5 order closure. The parameterization is implemented in a 3D transport model and tested against large eddy simulations of convective atmospheric boundary layers.

2.2 Formulation

We propose a parameterization to account for the concentration variability ($\overline{c'^2}$) that is based the conservation equation of the concentration variance. The latter reads:

$$\underbrace{\frac{\partial \overline{c'^2}}{\partial t}}_S + \underbrace{u_i \frac{\partial \overline{c'^2}}{\partial x_i}}_A = - \underbrace{2\overline{c'u'_i}}_G \frac{\partial \overline{c}}{\partial x_i} - \underbrace{\frac{\partial u'_i c'^2}{\partial x_i}}_T - \underbrace{\varepsilon_c}_D + \underbrace{2\overline{c'E'}}_E, \quad (2.1)$$

where u_i , c , E represent the wind components, the concentration and the emission. Equation (2.1) accounts for the time evolution of concentration variance (S) created by turbulent motion (T) and transported in 3D (A and G) space while it is dissipated (D). It contains an extra term that accounts for the contribution to the variance production originating from the surface spatial variability of the emissions. In order to solve (2.1) for the variance we need to close some of the terms. While terms G , T and D can be closed conventionally by using well assessed parameterizations (see Appendix), for the term E we propose the following expression,

$$\overline{c'E'} = r \left(\overline{c'^2} \right)^{1/2} \left(\overline{E'^2} \right)^{1/2}, \quad (2.2)$$

where r is the correlation coefficient between the concentration and the emission variances.

2.3 Methodology

Our method is based on using two models with different physical assumptions:

- (1) A Reynold Averaged Navier-Stokes (RANS) equation model that assumes an instantaneous and homogeneous mixing i.e. does not solve turbulence; and
- (2) a 3D Large Eddy Simulation (LES) model that explicitly solves the heterogeneity of mixing by the turbulent characteristics of the atmosphere.

The RANS model hosts the parameterization developed to account for the sub-grid emission variability and the concentration variance. We use for this purpose the Finite Volume Model (FVM) developed by Martilli (2002) Martilli et al. (2002). The LES code (Cuijpers and Duynkerke, 1993) generates all the control runs used to test the parameterization. When the 3D results of a LES are averaged according to the x and y directions and time they can be reduced to a vertical profile that coincides with a solely 1D-column of the 3D-RANS model.

With the LES code, we simulate a dry convective boundary layer over a domain of $10 \times 10 \times 1.5 \text{ km}^3$ with vertical and horizontal resolutions of 25 and 100 m, respectively, leading to $100 \times 100 \times 60$ grid-points simulation. For the wind and the potential temperature, periodic lateral boundary conditions are assumed. The maximal time step used is 0.5 s. The surface sensible heat flux is 0.05 K m s^{-1} . The geostrophic wind is set equal to 5 m s^{-1} , and the initial potential temperature profile has a constant value of 288 K below 662.5 m and increases by 0.6 K every hundred meters above this height.

The domain is divided into 4 sub-domains of $5 \times 5 \text{ km}^2$, in which statistics is calculated at each time step. In one of these sub-domains we have two centred emission scenarios where the surface of the emission is equal to 64 and 16% of the sub-domain area. The sources have different surface dimensions but emit the same quantity of mass (see Fig. 2.1).

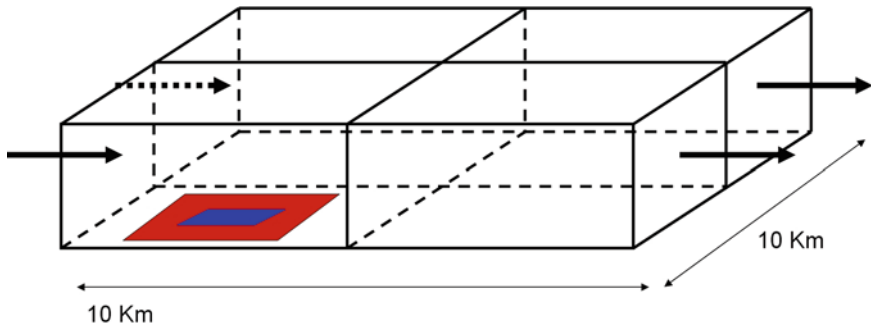
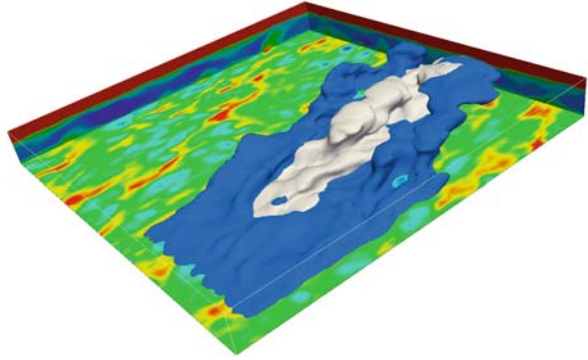


Fig. 2.1 Schematic representation of the modelling set-up. The *red* and *blue* areas represent the emitting surfaces of the two emission scenarios

Fig. 2.2 Instantaneous contour plot of the concentration fields for the two emission scenarios (64% in blue and 16% in grey) after two hours of simulation and with a threshold of 0.1 ppb. The potential temperature is also shown as coloured surfaces (See also Colour Plate 4 on page 172)



An instantaneous contour plot of the concentration fields for the two emission scenarios after two hours of simulation is shown in Fig. 2.2. The two plumes generated by the two emission patterns can be distinguished (blue and grey contours). The contours show clearly the squared shape of the emission pattern and its advection to the right of the domain.

The simulation runs for 2 h after a pre-run of 1 h for the dynamics only. The scalars have no initial concentrations in the atmospheric boundary layer (ABL). They are emitted from the surface with an emission rate of 0.1 ppb s^{-1} . Statistics are calculated for the last hour.

Using FVM we simulate the same ABL over the same domain, but using a horizontal mesh of 2×2 grid cells. The code is initialized with the results of the pre-run of 1 h performed by LES.

Let us assume that within a RANS grid cell of $5 \times 5 \text{ km}^2$ (coinciding with the LES sub-domain size with a resolution of $100 \text{ m} \times 100 \text{ m}$) we have a source with finite dimensions. The normal practice would be to average the emission from the source over the grid cell size and to use it as source term to solve the average concentration equation in order to account for the atmospheric dispersion. In our case, we take into account the variability of the source by including (2.2) into (2.1) and solving (2.1). The emission variances are calculated from the high-resolution emission inventory (used for the LES simulation); the parameter from r is deduced from the LES simulation and the concentration variance is calculated in a straight-forward manner.

2.4 Results

Figure 2.3 shows the result of the comparison between the LES variance and the RANS model variance for the 64% Emission Surface/Grid-Cell scenario in the four sub-domains. The agreement in the sub-domain where the emission takes place is excellent. However, results deteriorate for the other cells where the variances are

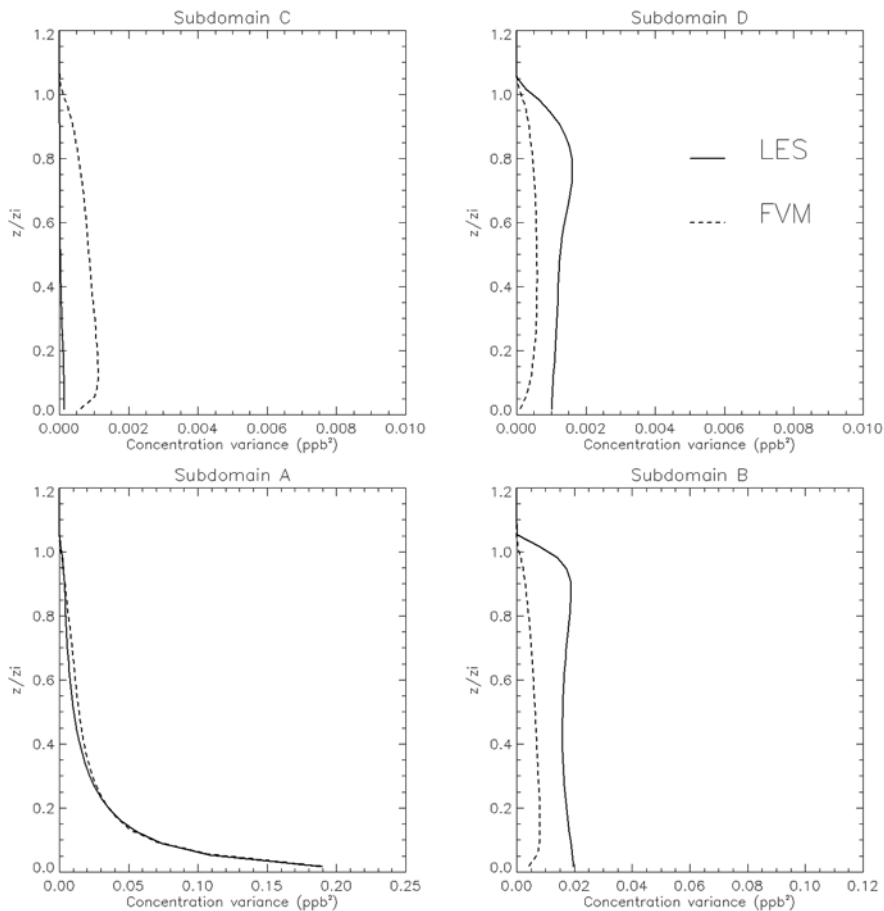


Fig. 2.3 Comparison of LES results with the RANS model (for different subdomains A–D) for the concentration of the 64% Emission Surface/Grid-Cell Surface scenario

only transported and dissipated. This is likely to be due to the lack of resolution in advection schemes since only a few grid points are considered.

From the beginning, we assumed that the LES represented true atmospheric motion due to its high resolution and accuracy in simulating atmospheric flow and dispersion. Within the LES domain we introduce 10 virtual measuring locations (Fig. 2.4) to investigate how the use of the emission variance parameterization will improve 3D RANS model results when compared with instantaneous measurements collected at 10 points (1–10) in Fig. 2.4.

Figure 2.5 shows the time evolution of concentration sampled at 12.5 m for the two emission patterns at 10 locations. The data are instantaneous concentration values produced by the LES with a 5 minute frequency. The thick black lines are the concentrations obtained from the 3D model whereas the shading is correspond

Fig. 2.4 Position of ten virtual sampling locations where time profiles of the concentrations for the two emission cases have been extracted

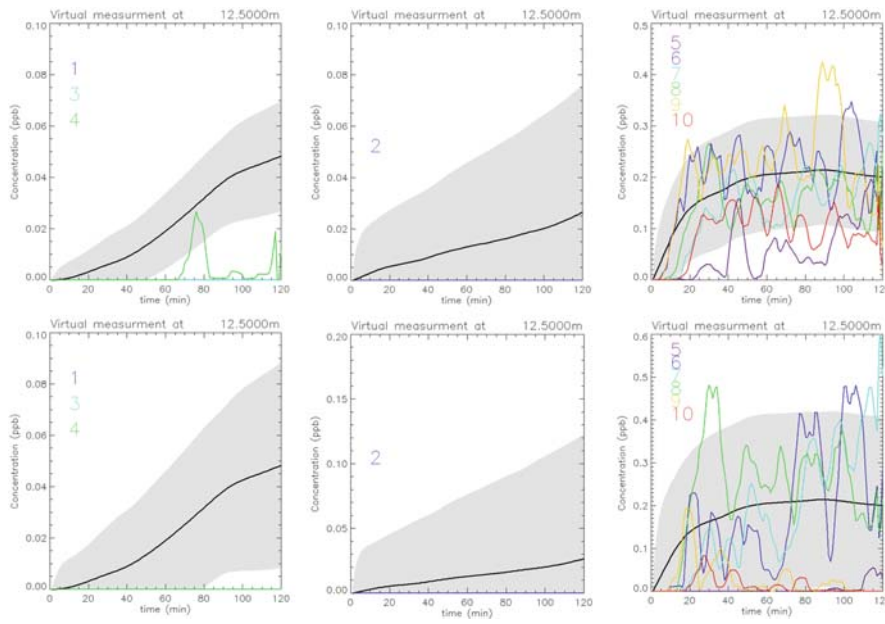
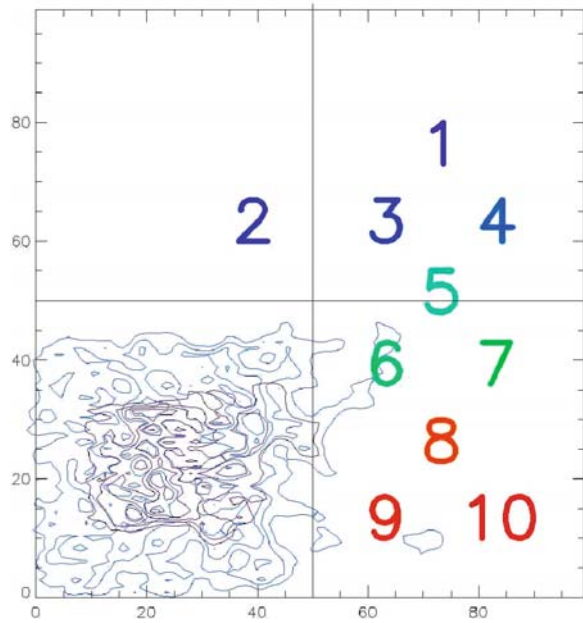


Fig. 2.5 Time profiles of the instantaneous concentrations sampled at 12.5 m and at the 10 locations (Fig. 2.4). The *thick black lines* show the average concentration obtained by the FVM model. The *shading* is the variance calculated with the new formulation. (*Upper*) 64% Emission Surface/Grid-Cell Surface case. (*Lower*) 16% Emission Surface/Grid-Cell Surface scenario (See also Colour Plate 5 on page 173)

to ± 1 standard deviation (note, values below 0 have been discarded as meaningless). As seen the 3D model results can be better compared with those of the LES, despite differences in the modelling approaches. Even with the extreme case of comparing instantaneous equations with Reynolds Averaged ones, when we consider the spatial variability of the emissions we can generalize the results of the RANS model.

2.5 Conclusions

A simple method to account for variability of emission has been proposed. The RANS model results compared to LES model are very encouraging. The parameterization will allow error bars to be added to model results. The next step will consider the analysis of different and more complex emission patterns and the refinement of information on the spatial variability.

Appendix: Other Closures Used for Prognostic Equation for the Variance of Pollutant Concentration

A description of the other closures used to solve the prognostic equation for the variance of pollutant concentration is given.

The turbulent fluxes of (G) (2.1) are calculated for the eddy covariance $\overline{(w'c')}$

$$\overline{w'c'} = -\frac{K_z}{\text{Pr}} \frac{\partial \bar{c}}{\partial z} \quad (2.3)$$

where the turbulent coefficient K_z is estimated using a K-1 closure (Bougeault and Lacarrère, 1989; Bélair et al., 1999), w is the vertical velocity, and Pr is the Prandtl number. In this closure a prognostic equation for the turbulent kinetic energy (TKE) e is solved, and turbulent coefficients and TKE dissipation are derived using length scales as follows:

$$K_z = c_k l_k e^{1/2} \quad (2.4)$$

$$\varepsilon_e = c_\varepsilon \frac{e^{3/2}}{l_\varepsilon} \quad (2.5)$$

The lengths l_k and l_ε are calculated at a particular level from the possible upward and downward displacements (l_{up} and l_{down}) that air parcels with kinetic energy e originating from the level z could accomplish before being stopped by buoyancy. In the following β is the buoyancy coefficient.

$$\int_z^{z+l_{up}} \beta (\theta(z) - \theta(z')) dz' = e(z) \quad (2.6)$$

$$\int_{z-l_{down}}^z \beta (\theta(z') - \theta(z)) dz' = e(z) \quad (2.7)$$

Therry and Lacarrère (1983) proposed a relation between l_k and l_ε

$$l_k = \left(1 + \frac{g}{\theta} \frac{\overline{w'\theta'}}{c_\varepsilon e^{3/2}} l_\varepsilon \right) l_\varepsilon \quad (2.8)$$

Bélair et al. (1999) used the budget equation for the TKE to derive the relation neglecting the turbulent transport contribution and assuming steady-state. This leads to

$$l_k = \left(1 + \frac{B_e}{D_e} \right) l_\varepsilon \quad (2.9)$$

or

$$l_k = \left(\frac{2B_e + G_e}{B_e + G_e} \right) l_\varepsilon \quad (2.10)$$

where B_e , D_e and G_e are the buoyancy, the dissipation and the gradient terms of the TKE budget equation. l_k is determined as the minimum between l_{up} and l_{down} (Bougeault and Lacarrère, 1989).

The turbulent transport T of (2.1) can be written as

$$\frac{\partial \overline{u'_i c'^2}}{\partial x_i} = -\frac{\partial}{\partial z} \left(\frac{K_z}{Pr} \frac{\partial \overline{c'^2}}{\partial z} \right) \quad (2.11)$$

The dissipation D of (2.1) can be written as

$$\varepsilon_{\overline{c'^2}} = \frac{\overline{c'^2}}{\tau_{\overline{c'^2}}} \quad (2.12)$$

Verver et al. (1997) used the TKE dissipation timescale divided by 2.5 as variance dissipation timescale to be inserted in the expression of the scalar variance dissipation. Using this expression with (2.5) leads to

$$\varepsilon_{\overline{c'^2}} = 2.5 c_\varepsilon \frac{e^{3/2}}{l_\varepsilon} \overline{c'^2} \quad (2.13)$$

C_ε and C_k are set to 0.125 and 0.7 and the Prandtl number Pr is 1/1.3. Boundary conditions for the TKE and the variances are calculated assuming no gradients across the surface.

References

- Bélair, S., Mailhot, J., Strapp, J.W., and MacPherson, J.I.: An examination of local versus nonlocal aspects of a TKE-based boundary-layer scheme in clear convective conditions. *Journal of Applied Meteorology*, 38, 1499–1518, 1999.
- Bougeault, P., and Lacarrère, P.: Parameterization of orography-induced turbulence in a mesobeta-scale model. *Monthly Weather Review*, 117, 1872–1890, 1989.
- Cuijpers, J.W.M., and Duynkerke, P.G.: Large eddy simulations of trade wind with cumulus clouds. *Journal of the Atmospheric Sciences*, 50, 3894–3908, 1993.
- Martilli, A.: Numerical study of urban impact on boundary layer structure: sensitivity to wind speed, urban morphology, and rural soil moisture. *Journal of Applied Meteorology*, 41, 1247–1266, 2002.
- Martilli, A., Clappier, A., and Rotach, M.: An urban surface exchange parameterisation for mesoscale models. *Boundary-Layer Meteorology*, 104(2), 261–304, 2002.
- Therry, G., and Lacarrère, P.: Improving the eddy kinetic energy model for planetary boundary layer description. *Boundary-Layer Meteorology*, 25, 63–88, 1983.
- Verver, G.H.L., Van Dop, H., and Holtslag, A.A.M.: Turbulent mixing of reactive gases in the convective boundary layer. *Boundary-Layer Meteorology*, 85, 197–222, 1997.

Meteorological and Air Quality Models for Urban Areas
Baklanov, A.; Grimmond, S.; Mahura, A.; Athanassiadou,
M. (Eds.)
2009, XVIII, 184 p. 38 illus., 14 illus. in color., Softcover
ISBN: 978-3-642-00297-7